[4]-Cyclo-2,7-carbazole as host material in high-efficiency phosphorescent OLEDs: A new perspective for nanohoops in organic electronics

Clement Brouillac, Fabien Lucas, Denis Tondelier, Joëlle Rault-Berthelot, Christophe Lebreton, Emmanuel Jacques, Cassandre Quinton, Cyril Poriel

[4]-Cyclo-2,7-carbazole as host material in high-efficiency phosphorescent OLEDs: A new perspective for nanohoops in organic electronics

Clément Brouillac,[a¥] Fabien Lucas,[b,¥] Denis Tondelier,[b] Joëlle Rault-Berthelot,[a] Christophe Lebreton,[c] Emmanuel Jacques,[c] Cassandre Quinton[a] and Cyril Poriel[a*]

[a] Univ Rennes, CNRS, ISCR-UMR 6226, F-35000 Rennes, France, [b] LPICM, CNRS, Ecole Polytechnique, IPParis, 91128 Palaiseau, France [c] Univ Rennes, CNRS, IETR-UMR 6164, F-35000 Rennes, France

email: cyril.poriel@univ-rennes1.fr

¥: equal contribution

Keywords: nanohoops, organic semiconductor, host material, phosphorescent organic light-emitting diode, structure-properties relationship, curved π-conjugated systems.

Abstract: In the last ten years, the development of π-conjugated nanohoops has been considerable owing to their remarkable properties. However, to date, their incorporation in organic electronic devices remains very scarce. In this work, we report the first high performance organic electronic device (*i.e.* Phosphorescent Organic Light-Emitting Diode PhOLED) incorporating a nanohoop ([4]-cyclo-*N*-butyl-2,7-carbazole **[4]C-Bu-Cbz**), revealing their potential in electronics. Thus, using the red phosphor $Ir(MDQ)_2(acac)$, the **[4]C-Bu-Cbz**-based PhOLED displays a high External Quantum Efficiency (EQE) of 17.0 %, a Current Efficiency (CE) of 20.6 $cd.A^{-1}$ and a Power Efficiency (PE) of 25.8 $lm.W^{-1}$ demonstrating that the charges injection, transport and recombination are particularly efficient. This performance is significantly higher than that of its linear counterpart, *N*-butyl-2,7-quartercarbazole **[4]L-Bu-Cbz**, which presents an EQE of 11.1 %, a CE of 13.0 $cd.A^{-1}$ and a PE of 15.7 $lm.W^{-1}$. The significant difference, in term of device performance, between cyclic and acyclic compounds provides a new basis to construct high-performance electronic devices. This study, which includes optical, electrochemical, morphological and charge transport properties, shows that nanohoops can be efficiently used as organic semi-conductors in electronics and opens the way to their practical uses in high-performance optoelectronic devices, which is now the next stage of their evolution.

The research field of hoop-shaped π-conjugated macrocycles, *i.e.* nanohoops, has significantly grown in recent years.[1] Besides their uncommon electronic properties induced by the radial distribution of the molecular orbitals,[2-7] and their recent applications in many different area[1], such as imaging tools in biology,[8] complexing agent for single-walled carbon nanotubes[9] or fullerenes,[10-12] carbon-based porous materials,[13, 14] or spin crossover compounds,[15] nanohoops are, over all, appealing π-conjugated materials, which can be potentially applied in electronic devices. However, this field of application remains a new ground to explore for nanohoops. Indeed, despite the fantastic development of organic electronic technologies in the last twenty years,[16, 17] there is only very few experimental data available on the integration of nanohoops in electronic devices, either Organic Light-Emitting Diodes (OLED),[18] Organic Field-Effect Transistors (OFET)[19, 20] or solar cells.[21, 22] This can be assigned to the difficulty to reach sufficient amount of nanohoops for device incorporation. The recent progresses in term of synthesis[20] start to change the deal and will surely allow nanohoops to go one-step further. Considering that linear π-conjugated systems are the molecular pillars, which have allowed the development of organic electronics, investigating their cyclic counterparts appears as an exciting challenge.[21, 23] Recently, the first detailed structure-properties-device performance relationship study of functional materials based on nanohoops *i.e.* [4]cyclo-*N*-alkyl-2,7-carbazoles has been reported in literature.[20] This work has shown how the supramolecular arrangement of the nanohoops affected their corresponding OFET characteristics. Field-effect (FE) mobility values of ca 10^{-5} $cm^2.V^{-1}.s^{-1}$ were recorded for cyclocarbazoles, whereas their non-bridged analogue [8]cyclo-*para*-phenylene **[8]CPP** did not display any FE mobility. In addition, this work has also shown that cyclocarbazoles-based devices were stable at the year time scale under inert atmosphere, and under electrical stress showing the real potential of these nanohoops in electronics. In the light of the importance of charge transport in all electronic devices,[24] these first data have shown that functional nanohoops can be used as organic semi-conductors (OSC). However, in this field, there is a long way to go in terms of fundamental knowledge and practical applications and to date, all the organic electronic devices incorporating a naonohoop display low performance. In the present work, we aim to go one-step further by reporting the first high-performance organic electronic device using a nanohoop. Thus, [4]-cyclo-*N*-butyl-2,7-carbazole, **[4]C-Bu-Cbz** cyclic assembly of four carbazole units substituted at C2 and C7, has been efficiently incorporated as a host material, in a red emitting phosphorescent OLED (PhOLED) using $Ir(MDQ)_2(acac)$ as emitter. This device displays a very high external quantum efficiency (EQE) of 17.0 %, a current efficiency (CE) of 20.6 $Cd.A^{-1}$, a power efficiency (PE) of 25.8 $lm.W^{-1}$ and a low threshold voltage (V_{on}) of 2.3 V. These performances translate excellent charges injection, transport and recombination. More importantly, in identical experimental conditions, its linear analogue, *N*-butyl-2,7-quartercarbazole **[4]L-Bu-CBz** (with the same C2/C7 linkages) presents significantly lower performance: EQE of 11.1 %, CE of 13.0 $cd.A^{-1}$ and PE of 15.7 $lm.W^{-1}$. Thus, this work shows not only that **[4]C-Bu-Cbz** can efficiently host a phosphorescent emitter within a PhOLED but also reveals, by comparison with its acyclic counterpart **[4]L-Bu-Cbz**, the strong advantages of cyclic *vs* linear structures. As the curvature of non-planar aromatic molecules is known to play a key role in achieving a desired function,[25] the present

finding can provide a new basis to construct high-performance electronic based on nanohoops.

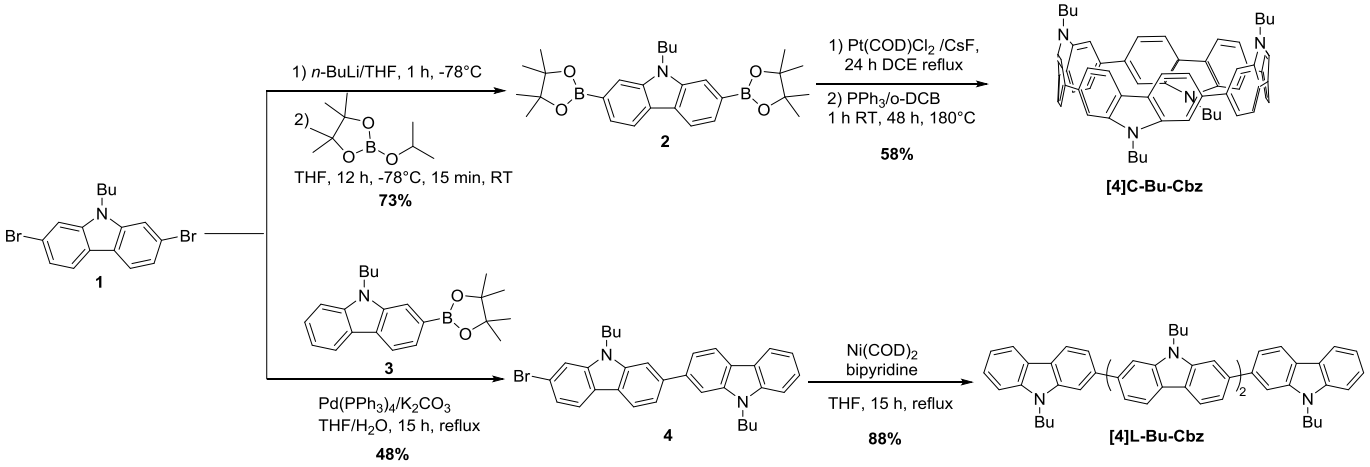

Figure 1. Synthesis of cyclic (**[4]C-Bu-Cbz)** and linear (**[4]L-Bu-Cbz**) quatercarbazoles.

One of the main weakness of nanohoops research field in materials science remains their synthesis, which has strongly hindered their development and especially electronic applications. Herein, **[4]C-Bu-Cbz** has been synthesized at the gram scale following optimized experimental conditions previously reported in literature (i.Pt(cod)Cl_2/CsF in DCE at 70°C for 24 h, ii. PPh_3 in *o*-DCB at RT for 1 h and at 180°C for 48 h), Figure 1. Compared to previous works,[20] this reaction has been scaled up by a factor 4 (1 g of starting material **2**) while maintaining an identical yield of 58%. As the scale-up is one of the inherent difficulty in nanohoop chemistry in general, this result appears beneficial for further application in materials science. The approach developed for linear *N*-butyl-2,7-quartercarbazole **[4]L-Bu-Cbz** is short, *i.e.* 2 steps, involves the same starting material (**1**) than that used for its cyclic analogue and displays an overall yield of 42% from **1**.

To insure efficient T_1/T_1 energy transfer from the host to the guest in a PhOLED, the energy level of the lowest triplet excited state (E_{T_1}) of the host material should be higher than that of the guest. However, the data on the phosphorescence properties of nanohoops remain very scarce.[26-29] These data are nevertheless crucial to define design rules of nanohoop-based host materials. At 77 K, in 2Me-THF, the emission spectrum of **[4]C-Bu-Cbz** displays two main contributions: the fluorescence contribution with a main band centred at 470 nm and the phosphorescence contribution with two bands at ca 548 and 584 nm (Figure 2A), providing a white light emission. The origin of these bands is ascertained by the gated emission as the fluorescence contribution is completely vanished. The decay curve for the band at 548 nm (λ_{exc} = 312 nm, Figure 2B) provides a very long lifetime of 0.65 s in accordance with an emission arising from the T_1 state. The E_{T_1} is measured at 2.26 eV from the maximum of the first phosphorescent band. The linear analogue **[4]L-Bu-Cbz** presents a blue shifted phosphorescent contribution spectrum with a main band detected at 520 nm, leading to an E_{T_1} value of 2.38 eV, higher to that of **[4]C-Bu-Cbz**. The lifetime of **[4]L-Bu-Cbz** is also significantly longer, 2.85 s, than that of **[4]C-Bu-Cbz**. Thus, the high strain of **[4]C-Bu-Cbz** (and nanohoops in general) leads to a decrease of both E_T and lifetime. One can hence conclude that the strain and the resulting deformations of the phenyl rings decrease the $E_{T1.}$ This is an interesting finding for further molecular designs. Theoretical calculations confirm this feature with an E_{T_1} evaluated at 2.20 eV for **[4]C-Bu-Cbz** and at 2.30 eV for **[4]L-Bu-Cbz**. The triplet spin density distribution (SDD, Figure 2C) is mainly located, for both molecules, on two connected carbazole units, but the contribution of the two other carbazoles is slightly more intense in the case of **[4]C-Bu-Cbz** than in **[4]L-Bu-Cbz**, in accordance with the higher value of the former. In 2020, Ruiz Delgado, Huang and their coworkers have reported the phosphorescence of a *meta*-linked [4]cyclo-3,6-carbazole.[30] Despite being a positional isomer of **[4]C-Bu-Cbz**, this macrocycle is flat and therefore structurally different. Its phosphorescent contribution, due to the *meta* linkages is blue shifted to 472 nm, leading to a strong increase of the E_{T_1}, measured at ca 2.63 eV. In addition, its linear analogue (3,6-quartercarbazole) has also been studied and presents an identical E_{T_1} of 2.63 eV (470 nm). So, there is no difference between the two *meta*-substituted quatercarbazoles and the cyclic *vs* linear nature does not significantly influence the T_1 state. In our case, **[4]C-Bu-Cbz** and **[4]L-Bu-Cbz** display a different behaviour as there is a difference of ca 0.12 eV between the two compounds in term of E_{T_1}. This highlights the influence of the strain on the T_1 state in nanohoops, which induces a significant difference compared to other macrocycles.

With an E_{T_1} of 2.26 eV, **[4]C-Bu-Cbz** can be used to host the red emitter $Ir(MDQ)_2acac$, which presents E_{T_1} values of 2.02/2.08 eV at room temperature/77 K.[31] Prior to device fabrication, a thin film of $Ir(MDQ)_2acac$, dispersed into either **[4]C-Bu-Cbz** or **[4]L-Bu-Cbz** (exactly corresponding to the EML of the PhOLED studied below) has been deposited on quartz by thermal evaporation. The resulting spectrum shows no trace of the emission of **[4]C-Bu-Cbz** / **[4]L-Bu-Cbz**, indicating an efficient energy transfer from the guest to the host (Figure 3A). In these conditions, the E_{T_1} of $Ir(MDQ)_2acac$, is measured at 2.01/2.02 eV from the peak maximum (Figure 3A), in full accordance with previous reports.[31]

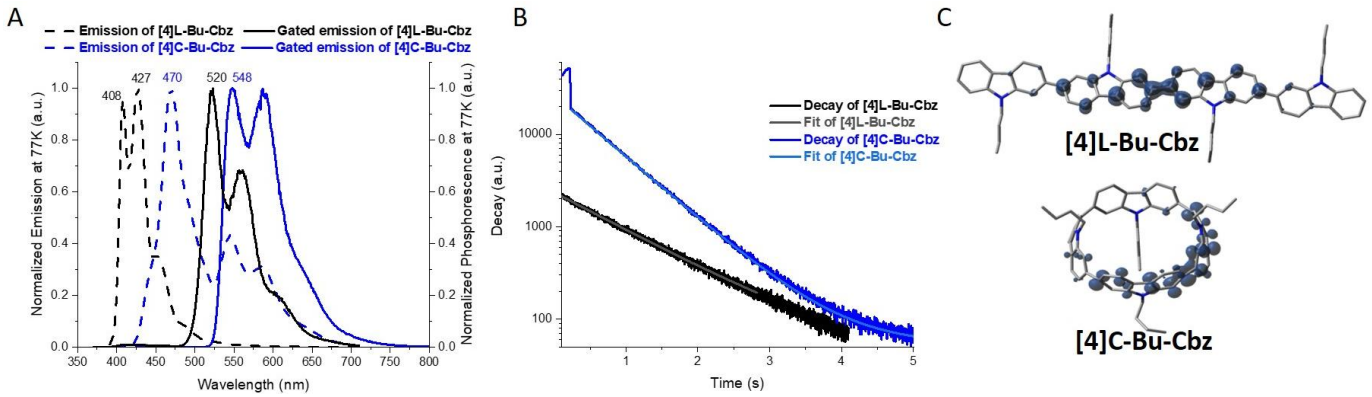

Figure 2. (A) Normalized emission and delayed emission at 77 K, in 2-Me-THF, of **[4]C-Bu-Cbz** (blue lines, λ_{exc}= 340 and 400 respectively) and of **[4]L-Bu-Cbz** (black lines, λ_{exc}= 360 nm for both); (B) Decay of **[4]C-Bu-Cbz** (λ_{exc}= 312 nm, λ_{em}= 543 nm) and **[4]L-Bu-Cbz** (λ_{exc}= 312 nm, λ_{em}= 520 nm); (C) Triplet spin density distribution: TD-DFT b3lyp 6-311+g(d,p).

The evaluation of defect density in the EML is a key point to obtain optimal recombination between hole and electron. This defect density is directly linked to the film organization and could be estimated by analysing charge transport. OFET electrical characterizations and I-V measurements in two-terminal devices have been performed to evaluate the charge transport properties of **[4]C-Bu-Cbz**[20] and **[4]L-Bu-Cbz** (See figures S17-S19). Note that charge transport studies of nanorings are almost absent from literature[19, 20, 32, 33] and comparison with linear analogues never reported to date. They nevertheless constitute the fundations of high efficiency devices First, the OFETs possessing a bottom-gate bottom-contact architecture (Figure S17[34]), in which the active layer is evaporated in the last step (in order to prevent structural defects resulting from the deposition of other layers[35, 36]) were used to extract the FE mobility. Used as active layer in such a type of device, **[4]C-Bu-Cbz** / **[4]L-Bu-Cbz** display mobility $\mu_{FE\text{-}sat}$ of 1.04×10^{-5} / 1.10×10^{-4} $cm^2.V^{-1}.s^{-1}$ in saturated regime (Figure S20, Table S6). In linear regime, the mobility $\mu_{FE\text{-}lin}$ of **[4]C-Bu-Cbz** remains identical, 1.03×10^{-5} $cm^2.V^{-1}.s^{-1}$, indicating that the linear mobility $\mu_{FE\text{-}lin}$ is almost unaffected by traps into the OSC. Oppositely, $\mu_{FE\text{-}lin}$ of **[4]L-Bu-Cbz** is significantly decreased compared to $\mu_{FE\text{-}sat}$ (3.48×10^{-5} *vs* 1.10×10^{-4} $cm^2.V^{-1}.s^{-1}$), showing the importance of traps in the layer organization. The ability to accumulate charges at the OSC/insulator interface is reflected through two key electrical parameters: the threshold voltage (V_{TH}, gate-source voltage needed for the channel to be populated) and subthreshold slope (SS, voltage required to increase the current at the OSC/insulator interface by one order of magnitude). The SS of **[4]C-Bu-Cbz** is significantly lower than that of **[4]L-Bu-Cbz**, 0.89 and 4.24 V/dec respectively. The V_{TH} values measured are also in accordance with this trend, -12.8 *vs* -20.6 V for **[4]C-Bu-Cbz** and **[4]L-Bu-Cbz** respectively (Table S6). These data fully corroborate those obtained with $\mu_{FE\text{-}lin}/\mu_{FE\text{-}sat}$ and suggest that the nanohoop promotes a better organization of the molecules in thin films whereas, in the linear oligomer, the density of structural defects is increased, which traps the charge carriers.

The carrier mobilities were also extracted in a two-terminal device by applying the Mott-Gurney model to the I-V measurements (space-charge-limited current SCLC transport, Fgure S18). The carrier mobility, $\mu_{carrier}$, was measured at 2.78×10^{-4} $cm^2.V^{-1}.s^{-1}$ for **[4]C-Bu-Cbz**, nearly two times higher than that of **[4]L-Bu-Cbz** (1.49×10^{-4} $cm^2.V^{-1}.s^{-1}$), Table S6. Note that the hole mobility of **[4]C-Bu-Cbz** is also significantly higher by one decade to that very recently reported for a nanohoop incorporating graphenic hexabenzocoronene unit.[33] More interestingly, the applied voltage needed to fill the traps (trap free region in SCLC model) in the case of **[4]L-Bu-Cbz** is higher, 28 V, than that needed, 19 V, in the case of **[4]C-Bu-Cbz**, confirming a higher trap density in the film made of [**4]L-Bu-Cbz**. From these studies, we can conclude that **[4]C-Bu-Cbz** displays better transport characteristics with less defects density than its linear analog **[4]L-Bu-Cbz**. This feature can be beneficial for the PhOLEDs investigated below.

Finally, red PhOLEDs (Figure 3) with the following architectures: ITO/Poly(3,4-ethylenedioxythiophene)-poly(styrenesulfonate) (PEDOT:PSS) (40 nm)/ 1,1-bis[(di-4-tolylamino)phenyl]cyclohexane (TAPC) (45 nm)/ 4,4′,4″-tris-(carbazol-9-yl)-triphenylamine (TcTa) (8 nm)/ **[4]C-Bu-Cbz** or **[4]L-Bu-Cbz**:$Ir(MDQ)_2(acac)$ (20 wt%, 20 nm)/1,3,5-tris(6-(3-(pyridin-3-yl)phenyl)pyridin-2-yl)benzene (TmPyPB) (55 nm)/Lithium fluoride (LiF) (1.2 nm)/Al (100 nm) were fabricated. PEDOT:PSS and LiF were selected as the hole- and electron-injection layers, and, TAPC and TmPyPB employed as the hole- and electron-transporting layers, respectively and TcTa as exciton-blocking layer. HOMO and LUMO energy levels of **[4]C-Bu-Cbz** (-5.18 / -2.40 eV[20]) and **[4]L-Bu-Cbz** (-5.30 / -2.17 eV) were obtained by cyclic voltammetry (Figure S14), those of TAPC, TcTa and TmPyPB were taken from literature (see Figure S16 for molecular structures).[37]

First, regarding the optical properties, no contribution of the host is detected in the electroluminescent (EL) spectrum, the devices exhibiting a red emission arising exclusively from $Ir(MDQ)_2acac$ (Figure 3C). This confirms good excitons transfer from the matrix to the dopant with both **[4]C-Bu-Cbz** and **[4]L-Bu-Cbz**. The EL spectrum of the device is identical to the thin-film one presented above (Figure 3A), showing the similitude of the radiative deactivation processes involved.

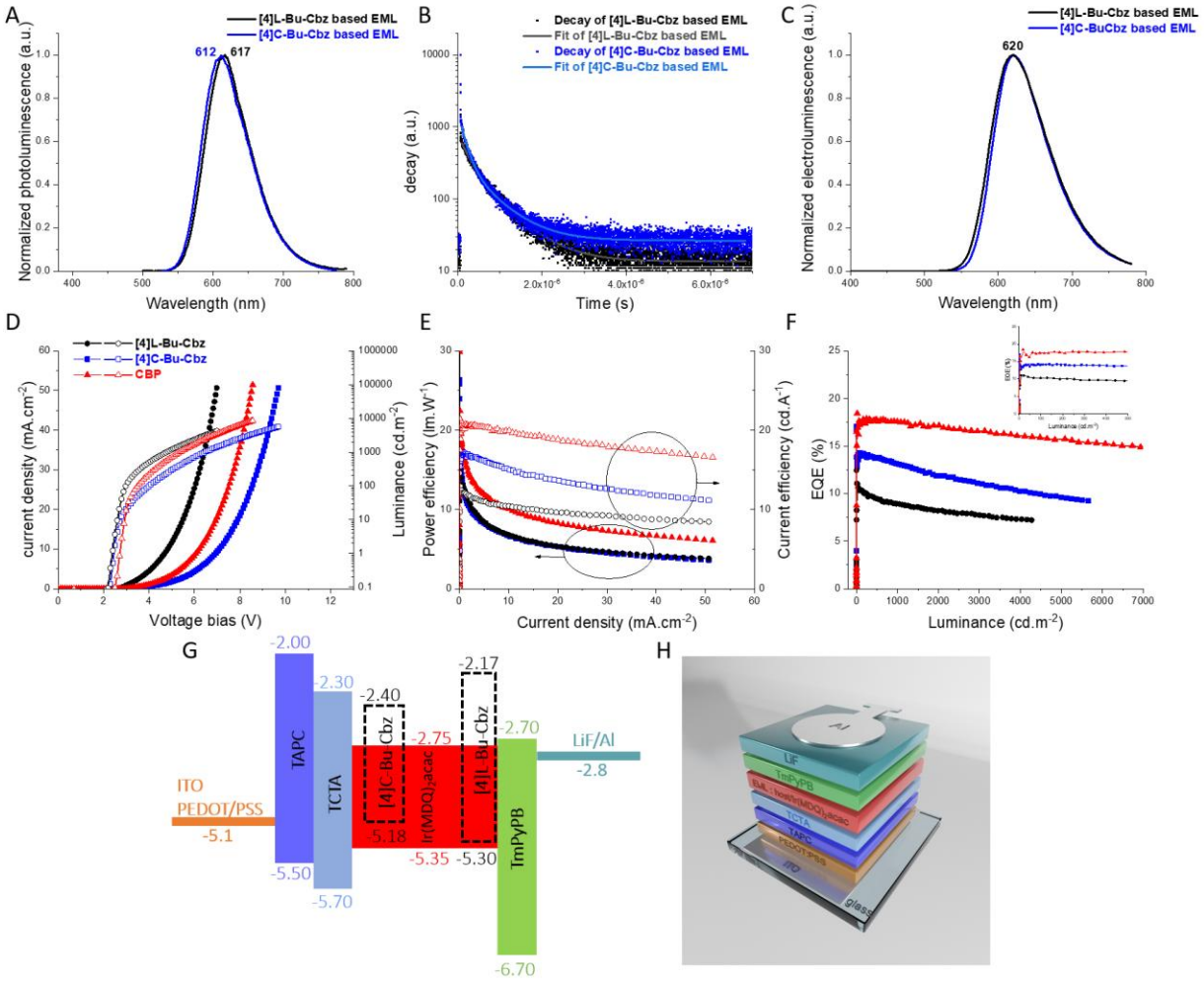

Figure 3. Normalized steady state photoluminescence, λ_{exc} = 400 nm (A), and time-resolved photoluminescence, λ_{exc} = 310 nm , λ_{em} = 650 nm (B), of 20 % doped $Ir(MDQ)_2acac$ into **[4]L-Bu-Cbz** or into **[4]C-Bu-Cbz**. Normalized electroluminescence spectra (C) and performances: Current density and luminance as a function of the bias voltage (D); power efficiency and current efficiency as a function of the current density (E); Roll-off EQE as a function of the luminance (F) of red PhOLEDs using as host matrix either **[4]C-Bu-Cbz** (blue lines), **[4]L-Bu-Cbz** (black lines) or **CBP** (red lines). Schematic representations of the PhOLED stack used in this work (G and H).

Table 1. PhOLEDs characteristics using as host matrix either **[4]C-Bu-Cbz**, **[4]L-Bu-Cbz** or **CBP**.

Host	V_{ON} (V)	EQE (%)	CE ($cd.A^{-1}$)	PE ($lm.W^{-1}$)	EQE (%)	CE ($cd.A^{-1}$)	PE ($lm.W^{-1}$)	CIE coordinates (x ; y)
		At 10 $mA.cm^{-2}$			Max (at J ($mA.cm^{-2}$))			At 10 $mA.cm^{-2}$
[4]C-Bu-Cbz	2.3	12.6	15.1	6.8	17.0 (0.01)	20.6 (0.01)	25.8 (0.01)	0.65 ; 0.35
[4]L-Bu-Cbz	2.2	8.9	10.4	6.8	11.1 (0.07)	13.0 (0.07)	15.7 (0.07)	0.65 ; 0.35
CBP	2.5	17.2	19.9	10.1	18.4 (0.08)	21.4 (0.08)	22.4 (0.08)	0.65 ; 0.35

[4]C-Bu-Cbz as host in $Ir(MDQ)_2acac$-based device (Figure 3D-F, blue lines) displays a very high EQE of 17 % (at 0.01 $mA.cm^{-2}$) with a low threshold voltage (V_{ON}) of 2.3 V. The corresponding current (CE_{max}) and power (PE_{max}) efficiencies are measured at 20.6 $cd.A^{-1}$ / 25.8 $lm.W^{-1}$ at 0.01 $mA.cm^{-2}$. These data translate the efficiency of this device in terms of charges injection, transportation, and recombination, showing the efficiency of **[4]C-Bu-Cbz** as a host. Interestingly, **[4]L-Bu-Cbz** was also incorporated as a host with the same device architecture, displaying significantly lower performances. Indeed, the EQE_{max} is measured at 11.1 %, CE_{max} at 13.0 $cd.A^{-1}$ and PE_{max} at 15.7 $lm.W^{-1}$ (at 0.07 $mA.cm^{-2}$), Figure 3D-F, black lines. At higher current densities, 10 $mA.cm^{-2}$, the EQE of **[4]C-Bu-Cbz** remains significantly higher than that of **[4]L-Bu-Cbz**: 12.6 % *vs* 8.9 %. These data demonstrate that **[4]C-Bu-Cbz** allows a better charge injection from adjacent layers to the EML and excitons transfer within the EML than **[4]L-Bu-Cbz**. Moreover, as shown with the charge transport studies, the intrinsic lower trap density of **[4]C-Bu-Cbz** *vs* **[4]L-Bu-Cbz** might help to increase the ratio of charge recombination and extraction of photons.

To interpret the different performances, phosphorescence lifetimes of the EMLs were first investigated (Figure 3B). The EMLs were exactly those used in the above mentioned PhOLEDs (20 wt% $Ir(MDQ)_2acac$). **[4]C-Bu-Cbz** and **[4]L-Bu-Cbz** based EMLs display radiative deactivation lifetimes of 0.47 and 0.57 µs at 650 nm, respectively. Thus, one can note that the lifetime is shorter for **[4]C-Bu-Cbz** than for **[4]L-Bu-Cbz**, which might help to reduce the triplet states density and the possibility of triplet-triplet annihilation (TTA),[38-42] resulting in higher device performances. The link between short deactivation of the EML and the efficiency of the device has been recently shown and is a key parameter in PhOLED efficiency.[37]

To gain insight into the surface morphology, AFM studies have been performed on the PhOLED active layer with the same stack (PEDOT-PSS, 40 nm)/TAPC, 45 nm/ TcTa, 8 nm/ **[4]C-Bu-Cbz** or **[4]L-Bu-Cbz**: $Ir(MDQ)_2acac$ 20 wt%, 20 nm, Figure 4) in order to well visualize the interface effects. This study reveals equivalent film roughness for both **[4]L-Bu-Cbz** and **[4]C-Bu-Cbz** with root mean surface roughness R_q of 0.57 and 0.59 nm respectively (Table S7). Maximum vertical distance between the highest and lowest peak is also equivalent with R_{max} values of 4.8 and 4.3 nm respectively. The interface between the TcTa and the emissive layer is then not responsible in the different PhOLEDs performances. Focusing on the general aspect of AFM images, **[4]C-Bu-Cbz** film is nevertheless smoother than that of **[4]L-Bu-Cbz** with spreading peaks. This feature could be linked to larger grain sizes and thus less defects density into **[4]C-Bu-Cbz** film than into **[4]L-Bu-Cbz**, in accordance with the higher performance of the former.

Another important feature arises from molecular orbital alignment in the device. Indeed, **[4]C-Bu-Cbz** displays a lower LUMO level than **[4]L-Bu-Cbz** (-2.40 *vs* -2.17 eV) leading to a better alignment with the LUMO of the electron transporting layer, TmPyPB (-2.70 eV). This characteristic is also surely involved in the higher performance obtained for the nanohoop. It is known for CPPs that their LUMO energy levels are lower than those of their linear analogues with the same number of phenyl units.[43] Herein, **[4]C-Bu-Cbz** and **[4]L-Bu-Cbz** display an identical trend. In PhOLEDs, this characteristic of nanohoops can be advantageously used to adjust the alignment of LUMOs, which in turn increases the performance.

Thus, the LUMO energy level, the organization of the active layer and the deactivation lifetime appear as first arguments to explain the higher performances of **[4]C-Bu-Cbz** *vs* **[4]L-Bu-Cbz**.

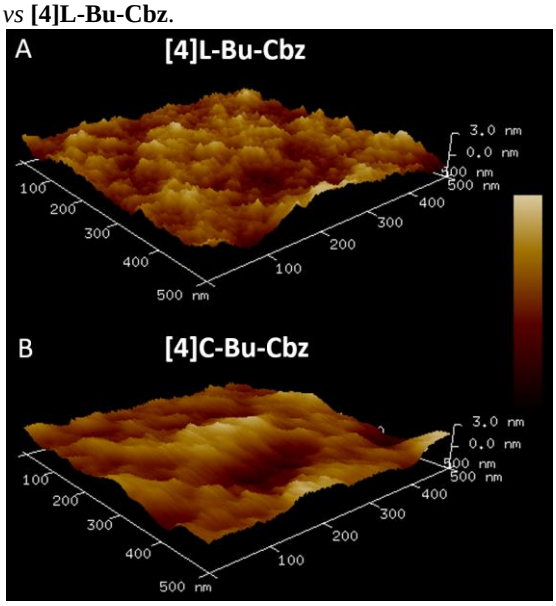

Figure 4. 2D ($500 \times 500 nm^2$) AFM images of (A) **[4]L-Bu-Cbz** and (B) **[4]C-Bu-Cbz.**

Finally, in order to evaluate the efficiency of **[4]C-Bu-Cbz** with state of the art materials, similar devices with the same architecture but using the well-known benchmark and efficient host, 4,4'-bis(*N*-carbazolyl)-1,1'-biphenyl, **CBP**, were investigated, Figure 3D-F and Table 1. **CBP** represents one of the most used commercially available host material for PhOLEDs incorporating $Ir(MDQ)_2acac$ as red phosphorescent guest.[44-46] Thus, an emissive layer constituted of **CBP** doped with $Ir(MDQ)_2acac$ leads to a device with a V_{ON} of 2.5 V, and EQE_{max} of 18.4 %, CE_{max} of 21.4 $cd.A^{-1}$ and PE_{max} of 22.4 $lm.W^{-1}$ at 0.08 $mA.cm^{-2}$. These performances are higher than those of **[4]C-Bu-Cbz** but nevertheless highlights the potential of nanohoops as host materials for PhOLEDs.

To summarize, we report herein the first high-performance electronic device using a nanohoop as active layer. Compared to its linear analogue **[4]L-Bu-Cbz**, **[4]C-Bu-Cbz** displays a lower E_{T1}, 2.26 *vs* 2.38 eV, showing the impact of the nanohoop strain on the E_{T1}. This unexpected finding reveals an unknown aspect of nanohoop that is the impact of strain on the phosphorescence properties. If the electronic properties of nanohoops start to be known especially for the flagship family of nanohoops CPPs, their applications, especially in organic electronics, remain almost unexplored. The charge transport studies also reveal better electrical properties for **[4]C-Bu-Cbz** *vs* **[4]L-Bu-Cbz**, due to a better organization of the film, highlighting a new appealing characteristic for nanohoops. Incorporated as host material in the EML of a PhOLED, **[4]C-Bu-Cbz** efficiently hosts the red phosphor $Ir(MDQ)_2acac$ with a high EQE of 17.0 %, a CE of 20.6 $cd.A^{-1}$ and a PE of 25.8 $lm.W^{-1}$. The PhOLED also displays a low V_{ON} of 2.3 V, translating a good charge injection. These performances are significantly higher than those of its linear analogue **[4]L-Bu-Cbz** (EQE = 11.1 %, a CE of 13 $cd.A^{-1}$ and a PE of 15.7 $lm.W^{-1}$), revealing the

influence of the cyclic *vs* linear geometry. These performances are already in the same range than those of benchmark materials such as **CBP** investigated herein. These findings show the potential of nanohoop structures in the emerging technologies of organic electronics. As the synthesis of nanohoops becomes now as efficient as linear ones (Figure 1), their use in electronics will continue to grow. With more accurate molecular designs, there is no doubt that the performance of nanohoops will also rapidly increase. By increasing the E_{T1}, green or even blue phosphors could be, for example, used. Recent works have shown that the nanohoop size has a significant impact on several electronic properties, *e.g.* HOMO and LUMO energies and fluorescence.[3, 7, 27, 47-53] [54] However, the evolution of E_{T1} as a function of the nanohoop size (and its resulting strain) is still in its infancy.[27-29]. This is a key step for further exploring materials designs, in order to tune E_{T1} of nanohoops, allowing in turn to fit the energy transfers within the PhOLEDs. This will deeply contribute to the development of nanohoops as organic materials for electronics. We are currently working in this direction.

Experimental Section

Experimental Details can be found in Supplementary Information.

Acknowledgements

This project has received funding from the European Union's Horizon 2020 research and innovation program under grant agreement No 699648 (FRODO). We thank GENCI (Project N°AD0100805032R1), the ANR (n°19-CE05-0024), the Agence de l'Environnement et de la Maitrise de l'énergie (ADEME) for PhD grant (CB), Dr Bruno Lafitte (ADEME), the CRMPO (Rennes). We also thank Dr B. Le Guennic (Rennes) for his help in theoretical calculations, Dr J.F Bergamini (Rennes) for the graphical abstract design and Dr Ludovic Favereau and Dr Julien Boixel (Rennes) for assistance in spectroscopy and Inorganic Theoretical Chemistry Team at ISCR (Rennes) for allocation of computational time.

References

[1]E. J. Leonhardt, R. Jasti, *Nat. Rev. Chem.* **2019**, *3*, 672-686.

[2]H. Omachi, Y. Segawa, K. Itami, *Acc. Chem. Res.* **2012**, *45*, 1378-1389.

[3]E. R. Darzi, R. Jasti, *Chem. Soc. Rev.* **2015**, *44*, 6401-6410.

[4]M. R. Golder, R. Jasti, *Acc. Chem. Res.* **2015**, *48*, 557-566.

[5]S. E. Lewis, *Chem. Soc. Rev.* **2015**, *44*, 2221-2304.

[6]S. Yamago, E. Kayahara, T. Iwamoto, *Chem. Rec.* **2014**, *14*, 84-100.

[7]Y. Segawa, A. Kukazawa, S. Matsuura, H. Omachi, S. Yamaguchi, S. Irle, K. Itami, *Org. Biomol. Chem.* **2012**, *10*, 5979-5984.

[8]B. M. White, Y. Zhao, T. E. Kawashima, B. P. Branchaud, M. D. Pluth, R. Jasti, *ACS Cent. Sci* **2018**, *4*, 1173-1178.

[9]K. Miki, K. Saiki, T. Umeyama, J. Baek, T. Noda, H. Imahori, Y. Sato, K. Suenaga, K. Ohe, *Small* **2018**, *14*, 1800720.

[10]T. Iwamoto, Z. Slanina, N. Mizorogi, J. Guo, T. Akasaka, S. Nagase, H. Takaya, N. Yasuda, T. Kato, S. Yamago, *Chem. Eur. J.* **2014**, *20*, 14403-14409.

[11]Y. Nakanishi, H. Omachi, S. Matsuura, Y. Miyata, R. Kitaura, Y. Segawa, K. Itami, H. Shinohara, *Angew. Chem. Int. Ed.* **2014**, *53*, 3102-3106.

[12]Y. Xu, R. Kaur, B. Wang, M. B. Minameyer, S. Gsänger, B. Meyer, T. Drewello, D. M. Guldi, M. von Delius, *J. Am. Chem. Soc.* **2018**, *140*, 13413-13420.

[13]H. Sakamoto, T. Fujimori, X. Li, K. Kaneko, K. Kan, N. Ozaki, Y. Hijikata, S. Irle, K. Itami, *Chem. Sci.* **2016**, *7*, 4204-4210.

[14]T. A. Schaub, E. A. Prantl, J. Kohn, M. Bursch, C. R. Marshall, E. J. Leonhardt, T. C. Lovell, L. N. Zakharov, C. K. Brozek, S. R. Waldvogel, S. Grimme, R. Jasti, *J. Am. Chem. Soc.* **2020**, *142*, 8763–8775.

[15]M. J. Heras Ojea, J. M. Van Raden, S. Louie, R. Collins, D. Pividori, J. Cirera, K. Meyer, R. Jasti, R. A. Layfield, *Angew. Chem. Int. Ed.* **2021**, *60*, 3515-3518.

[16]J. L. Bredas, S. R. Marder, *The WSPC References on Organic Electronics: Organic Semi-Conductors*, World Scientific

[17]Z.-Q. Jiang, C. Poriel, N. Leclerc, *Mater. Chem. Front.* **2020**, *4*, 2497-2498.

[18]Y.-Y. Liu, J.-Y. Lin, Y.-F. Bo, L.-H. Xie, M.-D. Yi, X.-W. Zhang, H.-M. Zhang, T.-P. Loh, W. Huang, *Org. Lett.* **2016**, *18*, 172-175.

[19]F. Lucas, L. Sicard, O. Jeannin, J. Rault-Berthelot, E. Jacques, C. Quinton, C. Poriel, *Chem. Eur. J.* **2019**, *25*, 7740-7748.

[20]F. Lucas, N. McIntosh, E. Jacques, C. Lebreton, B. Heinrich, B. Donnio, O. Jeannin, J. Rault-Berthelot, C. Quinton, J. Cornil, C. Poriel, *J. Am. Chem. Soc.* **2021**, *143*, 8804-8820.

[21]M. Ball, Y. Zhong, B. Fowler, B. Zhang, P. Li, G. Etkin, D. W. Paley, J. Decatur, A. K. Dalsania, H. Li, S. Xiao, F. Ng, M. L. Steigerwald, C. Nuckolls, *J. Am. Chem. Soc.* **2016**, *138*, 12861-12867.

[22]O. Koçak, I. P. Duru, I. Yavuz, *Advanced Theory and Simulations* **2019**, *2*, 1800194.

[23]M. Ball, C. Nuckolls, *ACS Cent. Sci* **2015**, *1*, 416-417.

[24]V. Coropceanu, J. Cornil, D. A. da Silva Filho, Y. Olivier, R. Silbey, J. L. Brédas, *Chem. Rev.* **2007**, *107*, 926-952.

[25]W.-S. Wong, M. Stępień, *Trends in Chemistry* **2022**, *4*, 573-576.

[26]K. Itami, H. Shudo, M. Kuwayama, M. Shimasaki, T. Nishihara, Y. Takeda, T. Kuwabara, A. Yagi, Y. Segawa, *ChemRxiv* **2021**, 1-6.

[27]M. Fujitsuka, C. Lu, B. Zhuang, E. Kayahara, S. Yamago, T. Majima, *J. Phys. Chem. A* **2019**, *123*, 4737-4742.
[28]D. A. Hines, E. R. Darzi, R. Jasti, P. V. Kamat, *J. Phys. Chem. A* **2014**, *118*, 1595-1600.
[29]D. A. Hines, E. R. Darzi, E. S. Hirst, R. Jasti, P. V. Kamat, *J. Phys. Chem. A* **2015**, *119*, 8083-8089.
[30]H. Zhu, I. Badía-Domínguez, B. Shi, Q. Li, P. Wei, H. Xing, M. C. Ruiz Delgado, F. Huang, *J. Am. Chem. Soc.* **2021**, *143*, 2164–2169.
[31]F. Lucas, C. Quinton, S. Fall, T. Heiser, D. Tondelier, B. Geffroy, N. Leclerc, J. Rault-Berthelot, C. Poriel, *J. Mater. Chem. C* **2020**, *8*, 16354-16367.
[32]E. Kayahara, L. Sun, H. Onishi, K. Suzuki, T. Fukushima, A. Sawada, H. Kaji, S. Yamago, *J. Am. Chem. Soc.* **2017**, *139*, 18480-18483.
[33]S. Wang, X. Li, K. Wei, X. Zhang, S. Yang, G. Zhuang, P. Du, *Eur. J. Org. Chem.*, *e202101493*.
[34]J.-D. Peltier, B. Heinrich, B. Donnio, O. Jeannin, J. Rault-Berthelot, E. Jacques, C. Poriel, *J. Mater. Chem. C* **2018**, *6*, 13197-13210.
[35]J.-D. Peltier, B. Heinrich, B. Donnio, E. Jacques, J. Rault-Berthelot, C. Poriel, *ACS Appl. Mater. Interfaces* **2017**, *9*, 8219-8232.
[36]S. Bebiche, P. Cisneros-Perez, T. Mohammed-Brahim, M. Harnois, J. Rault-Berthelot, C. Poriel, E. Jacques, *Mater. Chem. Front.* **2018**, *2*, 1631-1641.
[37]Q. Wang, F. Lucas, C. Quinton, Y.-K. Qu, J. Rault-Berthelot, O. Jeannin, S.-Y. Yang, F.-C. Kong, S. Kumar, L.-S. Liao, C. Poriel, Z.-Q. Jiang, *Chem. Sci.* **2020**, *11*, 4887-4894.
[38]A. Köhler, H. Bässler, *Mat. Sci. Eng. C- Reports* **2009**, *66*, 71-109.
[39]F. Steiner, J. Vogelsang, J. M. Lupton, *Phys. Rev. Lett.* **2014**, *112*, 137402.
[40]M. A. Baldo, C. Adachi, S. R. Forrest, *Phys. Rev. B* **2000**, *62*, 10967-10977.
[41]Y.-K. Wang, Q. Sun, S.-F. Wu, Y. Yuan, Q. Li, Z.-Q. Jiang, M.-K. Fung, L.-S. Liao, *Adv. Funct. Mat.* **2016**, *26*, 7929-7936.
[42]Q. Wang, Q.-S. Tian, Y.-L. Zhang, X. Tang, L.-S. Liao, *J. Mater. Chem. C* **2019**, *7*, 11329-11360.
[43]T. Iwamoto, Y. Watanabe, Y. Sakamoto, T. Suzuki, S. Yamago, *J. Am. Chem. Soc.* **2011**, *133*, 8354-8361.
[44]Y. L. Chang, Z. B. Wang, M. G. Helander, J. Qiu, D. P. Puzzo, Z. H. Lu, *Org. Electron.* **2012**, *13*, 925-931.
[45]J. P. Duan, P. P. Sun, C. H. Cheng, *Adv. Mater.* **2003**, *15*, 224-228.
[46]C. Zang, X. Peng, H. Wang, Z. Yu, L. Zhang, W. Xie, H. Zhao, *Org. Electron.* **2017**, *50*, 106-114.
[47]M. Fujitsuka, D.-W. Cho, T. Iwamoto, S. Yamago, T. Majima, *Phys. Chem. Chem. Phys.* **2012**, *14*, 14585-14588.
[48]R. Jasti, J. Bhattacharjee, J. Neaton, C. R. Bertozzi, *J. Am. Chem. Soc.* **2008**, *130*, 17646-17647.
[49]G. Povie, Y. Segawa, T. Nishihara, Y. Miyauchi, K. Itami, *J. Am. Chem. Soc.* **2018**, *140*, 10054-10059.
[50]L. Wang, S.-H. Chen, D. He, Q.-J. Li, Y.-L. Liu, M.-S. Wang, *J. Phys. Chem. C* **2020**, *124*, 11081-11091.
[51]H. Jia, G. Zhuang, Q. Huang, J. Wang, Y. Wu, S. Cui, S. Yang, P. Du, *Chem. Eur. J.* **2020**, *26*, 2159-2163.
[52]Y. Nakagawa, R. Sekiguchi, J. Kawakami, S. Ito, *Org. Biomol. Chem.* **2019**, *17*, 6843-6853.
[53]L. Sicard, F. Lucas, O. Jeannin, P. A. Bouit, J. Rault-Berthelot, C. Quinton, C. Poriel, *Angew. Chem. Int. Ed.* **2020**, *59*, 11066-11072.
[54]F. Lucas, J. Rault-Berthelot, C. Quinton, C. Poriel, *J. Mater. Chem. C* **2022**, *10*, 14000-14009.